Experimental Thermal and Fluid Science 45 (2013) 25–33

Contents lists available at SciVerse ScienceDirect

Experimental Thermal and Fluid Science

journal homepage: www.elsevier.com/locate/etfs

Droplet dispersion characteristics of the hollow cone sprays in crossflow

Haibin Zhang [a,b], Bofeng Bai [a,*], Li Liu [a], Huijuan Sun [a], Junjie Yan [a]

[a] State Key Laboratory of Multiphase Flow in Power Engineering, Xi'an Jiaotong University, Xi'an 710049, China
[b] School of Chemical Engineering and Technology, Xi'an Jiaotong University, Xi'an 710049, China

ARTICLE INFO

Article history:
Received 12 May 2012
Received in revised form 11 September 2012
Accepted 21 September 2012
Available online 3 October 2012

Keywords:
Hollow cone spray
Crossflow
Coherent structure
Mixing

ABSTRACT

The flows in a jet entering a crossflow are unsteady and the droplet movement is of vital importance for the two-phase mixing effect. In this paper, the hollow cone spray into the crossflow is investigated experimentally by using the PIV visualization system and the image-processing techniques. The experiments are carried out inside a rectangular duct (95 mm × 95 mm in cross-section) at the ambient temperature and pressure. Different nozzle injection angles and crossflow velocities are experimented on. The instantaneous droplet distributions and the velocity vector fields are obtained. Our results show that the flow field falls into three main domains and their effects on the movement and distribution of the droplet are varied. The coherent structure which breaks the stability of the upper counter-rotating vortex pair (CVP) structure is induced on the interface between the upper CVP and the mainstream zone. When the spray is against the crossflow the larger coherent structures are induced and impose greater influences on the mixing process. The turbulence intensity on the shear layer increases and the dispersion of the droplet is promoted. The experimental findings will benefit the understanding of the mixing mechanism of the hollow cone spray in the crossflow and the achievement of an optimum mixing.

1. Introduction

The liquid spray injected into a crossflowing airstream has found wide applications. Examples include film cooling for turbines, fuel injection for burners, secondary injection in rocket nozzles for thrust vector control in propulsive systems as well as in the research of V/STOL aircrafts, and high quality steam generation in steam generators for in situ thermal recovery of heavy oil (which has great application prospect in the future oil industry). In most of these cases, the jets enter at right angles to the mainstream. The non-uniform droplet distribution in the flow can significantly inhibit the efficiency of the evaporators in heat exchanges. Engineering applications require a more profound understanding of the resultant flow field with such mixing augmentation. For all the previous intensive researches, a complete knowledge still eludes researchers.

Analytical and experimental studies were carried out on the jets in crossflow, including the liquid jet [1–6], the airblast liquid jet [7–11] and the flat-fan spray jet [12–14]. The liquid breakup, flow field characteristics, droplet movement, two-phase interaction were investigated in details. The vortices such as the counter-rotating vortex pair (CVP), the leading vortex, the shear layer vortex and the multiple vortexes and their contribution to the mixing were obtained. In the mixing process, the dispersion of the droplet is a major factor for the evaluation of the mixing. The dispersion of the droplet is determined by the spray nozzle and the crossflow in the initial mixing stage and is affected by different scales of vortices occurring in the flow field in the later mixing stage. Studies confirm that the stable large-scale vortices can lead to the preferential concentration of the droplet and consequently result in the non-uniform droplet distribution. So how to control the droplet dispersion in order to achieve a desirable mixing is an important issue in the spray/crossflow study.

In the study on the hollow cone spray nozzle, the liquid first emerges in the form of a sheet which quickly disintegrates into droplets due to the aerodynamic instability in the 'break-up region' and which interacts strongly with the atmosphere. Just downstream in the 'spray region', the liquid is in the exclusive form of droplets. Considerable research efforts have been directed towards the investigation on the break-up region and just beyond [15–19]. But the studies on the dispersion of the droplets in a crossflow are relatively few. Ghosh and Hunt [20] developed an analytical model within all the practical ranges of the ratio of the jet speed to the crossflow speed to address the fundamental problem in the fluid mechanics about how fluid jets were deflected and deformed. Kachhwaha et al. [21,22] studied the movement and evaporation of the spray droplets in both the parallel and counter-flow configurations. They proposed a two-dimensional model which agreed well with the experimental results.

In the mixing chamber of a real engine, the mixing is commonly conducted in confined space and finite distance, which inevitably

* Corresponding author. Tel.: +86 29 8266 5316; fax: +86 29 8266 9033.
E-mail address: bfbai@mail.xjtu.edu.cn (B. Bai).

0894-1777/$ - see front matter Crown Copyright © 2012 Published by Elsevier Inc. All rights reserved.
http://dx.doi.org/10.1016/j.expthermflusci.2012.09.021

leads to the impingement of the spray onto the wall. This results in further complication of the three-dimensional flow and makes close observations and analysis difficult. The primary concern in the practical mixing is to achieve a desirable mixing within the distance as short as possible. Therefore, in the experiments we focus on the mixing process in the early stage over a relatively short distance. We find that the mixing is mainly determined by the large-scale vortices. Furthermore, due to the confined mixing flow field and the measurement technical limitations, it is quite hard to decide the micro-dynamic behavior of the individual droplet. In engineering applications, such major influencing parameters as nozzle atomization conditions, crossflow velocity and spray injection angle are our main consideration. Hence, the mixing flow field structure, the spray droplet group dispersion and the droplet preferential concentration caused by the large-scale vortices are given priority to in our studies.

In our previous flow visualization investigations [23,24], the transverse droplet distributions and the velocity vector distributions were obtained in different cross-sections along the crossflow direction. The mixing effect is analyzed from the view of the time-averaged droplet distribution, and the preliminary evaluation of the mixing quality is given. But this method can merely correctly reflect the uniformity of the distribution of droplets mathematically, but not spatially. In order to resolve this problem, the mixing should be investigated from the point of view of the profound mixing mechanism. In our recent research, the dynamic of the

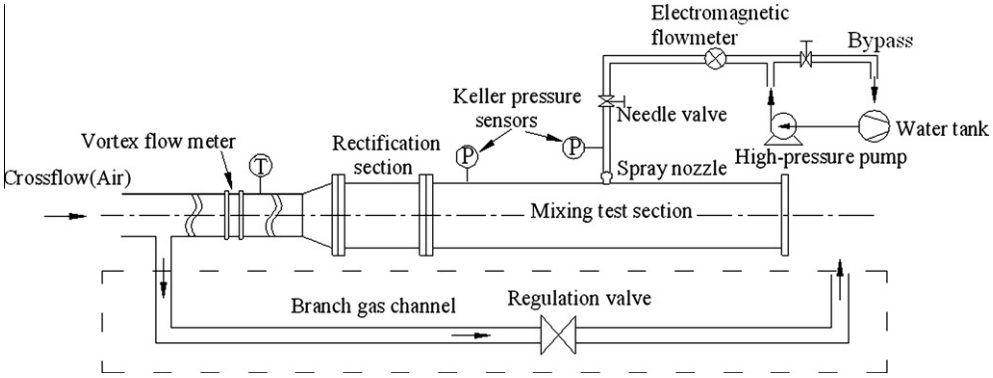

Fig. 1. Mixing system for a hollow cone sprays in crossflow.

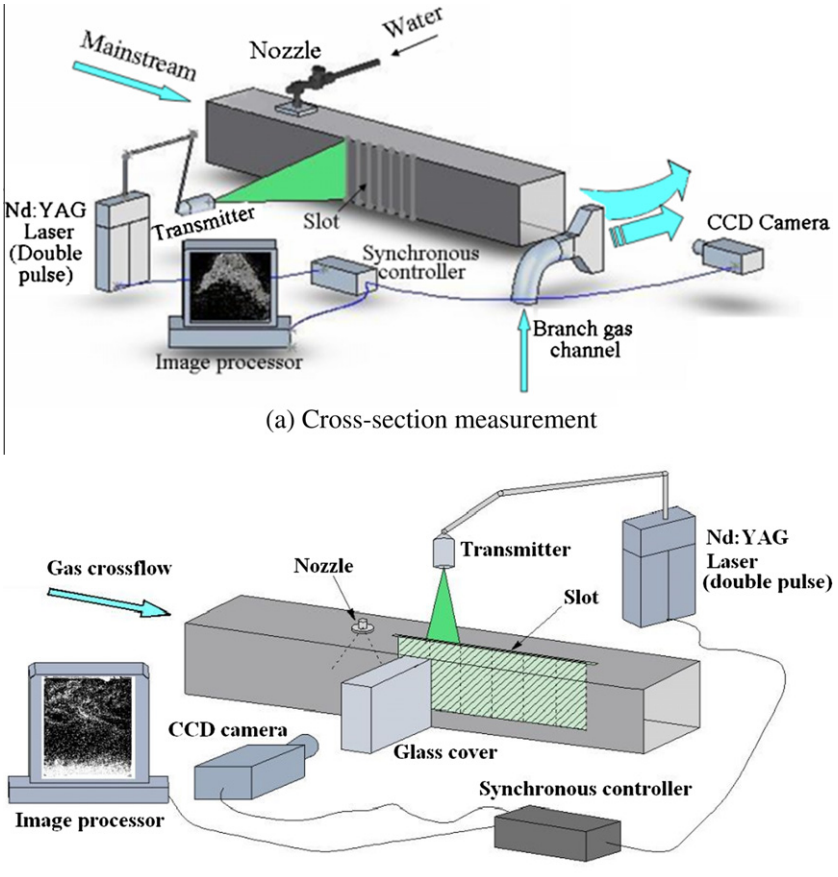

Fig. 2. Schematic diagram of the PIV measurement system.

large-scale vortices and the droplet dispersion are highlight. In this paper, we analyze the dynamic features of the droplets in the longitudinal sections, the characteristics of the large-scale vortices on different conditions and their influences on the droplet dispersion. We also discuss the influences of the spray injection angle on the droplet dispersion. This work will expected to help the research on the control of the mixing between the hollow cone spray droplets and the gas crossflow and have practical significance for the mixing chamber design and performance improvement in relevant industrial applications.

2. Experimental setup and method

2.1. Experimental system

The experimental system, as is shown in Fig. 1, consists of a gas loop, a water loop, a test section and a water tank. A long square duct (0.095 × 0.095 m in cross-section and 1.0 m in length) is used here corresponding to the practical engine structure. The duct supplies a filtered air stream through the wire mesh and honeycomb to avoid ambient disturbances. The Re numbers of the gas crossflow range from 25,700 to 45,000 with the relative turbulence intensity of less than 4.5%. The crossflow turbulence is so weak that it makes no significant addition to the spray turbulence. The discharged water from the pump passes via the flowmeter with the uncertainty of 1%, and then flows through the regulating valves and into the nozzle. The needle valve is located ahead of the nozzle to control the water flow rate precisely and ensure the stability of the water pressure. The mixing between the spray droplets and the crossflow is thus achieved in the test section.

Two sets of PIV testing are arranged here to measure the flow field in the cross-section and the longitudinal sections, respectively (see Fig. 2). The coordinate axes used to orient the measurements are centered at the nozzle orifice. The three mutually orthogonal directions (*X*, *Y*, and *Z*) are aligned as is shown in Fig. 3. To obtain the spray droplet distribution in the cross-sections, we install a branch gas channel to control the outlet flow direction and prevent the CCD lens from being polluted, as is shown in Fig. 2a. In the measurement of the droplet distribution in the longitudinal section, we use a glass cover ($W \times H \times L = 0.06 \times 0.095 \times 0.35$ m) to eliminate the influence of the liquid wall film on the side wall (see Fig. 2b). More details of the experiment are available in Bai et al. [23] and Liu et al. [25] in which the validity of the testing was included.

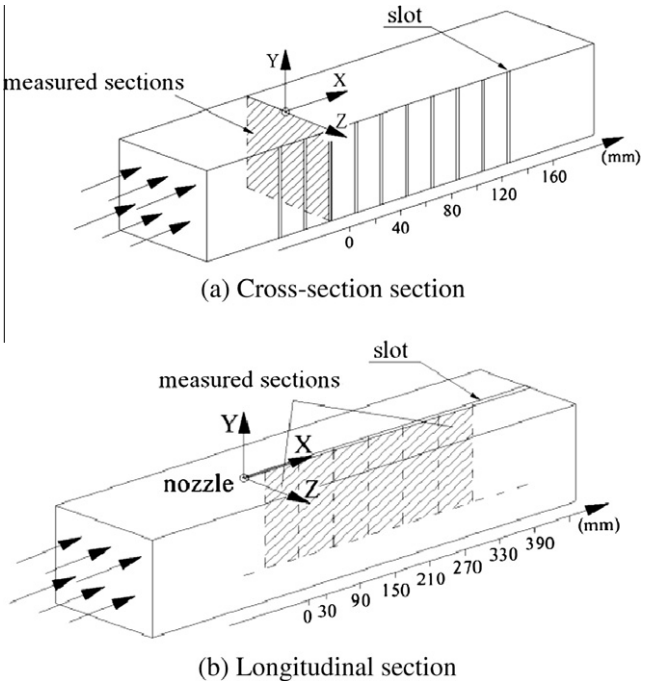

Fig. 3. Schematic drawing of the measurement sections.

Commercially available nozzles (1/4MK B80100S303-RW, H. Ikeuchi & Co., Ltd.) are used here (see Fig. 4). The diameter of the nozzle orifice is 0.5 mm. The volume flux is 0.03 m^3/h at the pressure of 0.7 MPa with the spray angle of 80°. The initial atomization droplet velocity is about 22.3 m/s with D_{32} (the Sauter Mean Diameter (SMD)) of 104 μm. The nozzle spray angle and the injection angle, denoted by α, are illustrated in Fig. 5. The nozzles are located 0.5 m downstream from the inlet of the test section.

The mean gas flow rate is measured with the vortex shedding flow meter with a variation of less than 2%. The mass flow of the water is measured with an electromagnetic flow meter. The Keller pressure sensors precisely control the pressure difference of the spray at a fixed value of 0.7 MPa. An NI data acquisition card records and stores the experimental data. The effects of the injection angles (60°, 75°, 90°, 105°, and 120°) and the crossflow velocity with the single nozzle on the mixing are investigated in the experiments. In order to validate the experimental results, we conduct three independent experiments on each testing condition. Detailed experimental conditions are shown in Table 1.

2.2. Flow visualization setup

We conduct the PIV measurements of the instantaneous velocities and distribution of the spray droplets using a TSI PIV processor

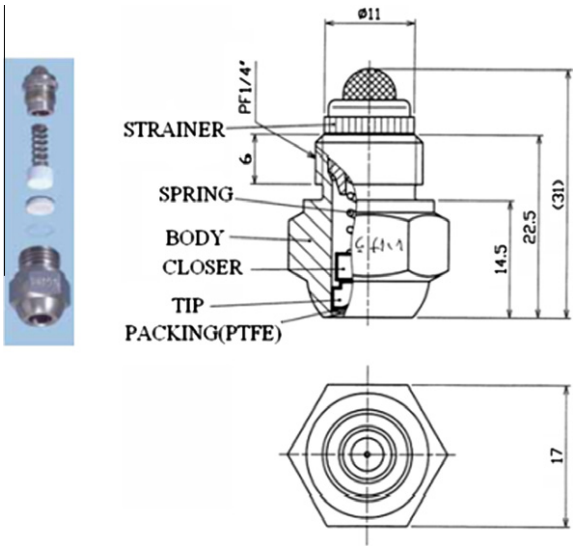

Fig. 4. Hollow cone nozzle (adopted from "The Mist Engineers", H. Ikeuchi & Co., Ltd.).

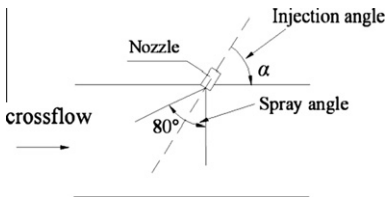

Fig. 5. Schematic drawing of the spray angle and the injection angle of the nozzle.

Table 1
Experimental conditions.

Number of nozzle	ΔP (MPa)	$\dot{m}_l$ (10^{-3} kg/s)	D_{32} (μm)	Re (gas)	Injection angle (α)
1	0.7	8.33	104	25700	60°, 75°, 90°, 105°, 120°
				32100	60°, 75°, 90°, 105°, 120°
				45000	60°, 75°, 90°, 105°, 120°

system with a Continuum Surelite Nd: YAG pulsed laser system (532 nm), capable of producing a 2×200 mJ, 8 ns laser pulses. The droplet-ladened flow is illuminated by the laser sheets (approximately 1 mm thick) aligned in the measurement sections of the spray droplets. The scattered light from the droplets is captured by the synchronized CCD camera with a CCD array size of 2048×2048 pixels. The scale factor calculated is about 55.7 μm/pixel. In the experiments, we get forty pairs of instantaneous images in each cross-section at five frames per second. In data processing, we use TSI FlowManager software and Tecplot and derive the velocity and vorticity fields.

3. Results and discussion

3.1. Analysis of the flow field

Fig. 6 and 7 show the spray droplet distribution and the droplet velocity vector in different cross-sections along the mixing flow field. It can clearly be seen that two large-scale CVP structures occur in the mixing flow field. The upper CVP structure is result of the pressure change. When a crossflow encounters the hollow cone spray, a 'shadow' of lower pressure appears behind the spray hollow cone. The surrounding air is entrained to the rear of the spray and then the upper CVP structure occurs. The bottom CVP structure is induced owing to the spray-wall impingement and the influence of the walls. Due to the confined channel, the initial spray droplets with larger momentum can penetrate the mainstream and reach the sidewall and then the droplet-wall impingement occurs. The flow field near the bottom wall becomes complex due to the impingement regimes of rebound, spread and splash. The crossflow will be forced to rotate under the combined effects of the shear stress caused by the high-speed spray droplets and the spray-wall impingement and thus the bottom CVP structure is formed. In the beginning, the bottom vortices form in the corner of the sidewall and then move toward the center and at the same time increase in size (see $x/D = 2.53$). As the mixing develops, the two CVP structures become increasingly unstable because of the interactions among them and the edges of the duct. The droplet dispersion is dominated by the CVP structures. They cause air to be entrained and then the small droplets are carried and pushed further by the entrained air. Due to the centrifugal effect, the droplets tend to accumulate along the edges of the vortex structures.

The primary concern in our study is to achieve a desirable mixing effect over the distance as short as possible. Experiments confirm that due to the larger droplet initial momentum and inertia, in the early stage of the mixing the large-scale CVP structures exert greater effect on the spray droplet dispersion than the secondary flow does. So the influence of the secondary flow on the droplet dispersion is ignored. Its well known that the stable large-scale turbulent structures which control the local particle contribution

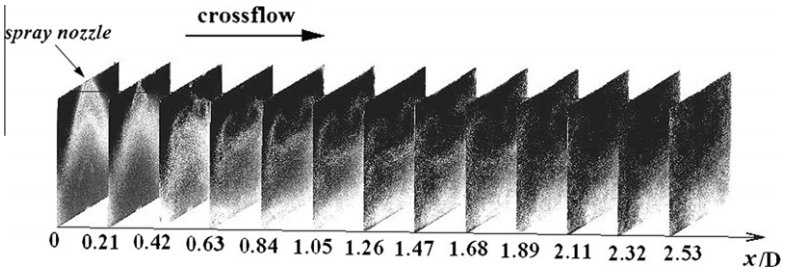

Fig. 6. Time-averaged images in each measured cross section for $\alpha = 90°$ (Re = 25700).

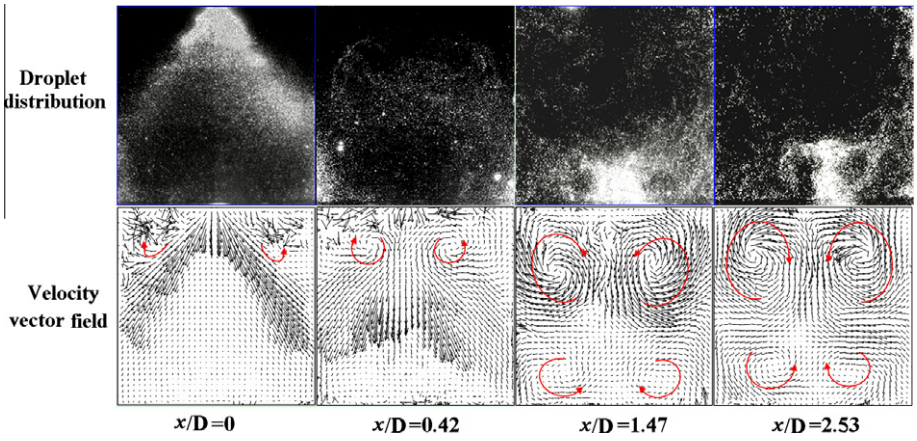

Fig. 7. Droplet distribution and velocity vector fields in different cross sections for $\alpha = 90°$ (Re = 25700).

and dispersion by convection can lead to the preferential concentration of the droplets and consequently result in non-uniform dispersion and concentrations in the flow. Hence, increasing the flow field disturbance to break the stability of the CVP is easy access to mixing enhancement. The present paper focuses on analyzing the dynamics of the upper CVP structure at different injection angles on the basis of the droplet distributions and movement features. This work is intended to extend and deepen our earlier flow visualization studies and explain why a better mixing effect is possible when $\alpha < 90°$.

In the instantaneous flow field measurement, the CVP structures remain stable near the nozzle but tend to become unstable with the enhanced disturbance along the mixing duct. Fig. 8 shows the instantaneous droplet distributions in the XOY longitudinal section on different conditions. Combining the spray droplet distributions in the cross-section and the central longitudinal section, we picture the mixing flow field of the hollow cone spray into the crossflow, as is shown in Fig. 9. According to the droplet distributions and the vortex structures, here we define the zone between the upper CVP and the bottom CVP as the mainstream zone in which the flow field is less affected by the CVP structures. So the flow field falls into three parts: the upper CVP zone, the mainstream zone and the bottom CVP zone. In Fig. 8, clearly it can be seen that on the interface of the upper CVP and the mainstream zone, the droplet distribution features an obvious coherent structure and along the mixing flow field the streamwise vortices increase in size gradually. For the three injection angles, the most obvious coherent structure occurs with $\alpha = 60°$, followed by $\alpha = 90°$, and the weakest coherent structure appears with $\alpha = 120°$. This observation indicates that the coherent structures occur in the gas-phase flow field and when the spray is against the crossflow, the induced coherent structures will become more obvious.

Furthermore, when $\alpha = 60°$, the central cross-section of the flow field is filled with the spray droplets. When $\alpha = 90°$, the obvious droplet clusters are induced. When $\alpha = 120°$, the spray droplets cluster in great numbers and in a large area at the bottom of the mixing duct. As the crossflow velocity increases, the droplet enrichment decreases and the region of high droplet concentration shrinks. In addition, with $\alpha = 90°$, most of the droplets distribute in the middle and the lower parts of the central section but few in the upper part at the lower crossflow velocity. As the crossflow velocity increases, the droplets move upwards and fill up the section gradually.

From the fluid dynamic point of view, when the nozzle spray is against the crossflow ($\alpha < 90°$), the interactions between the

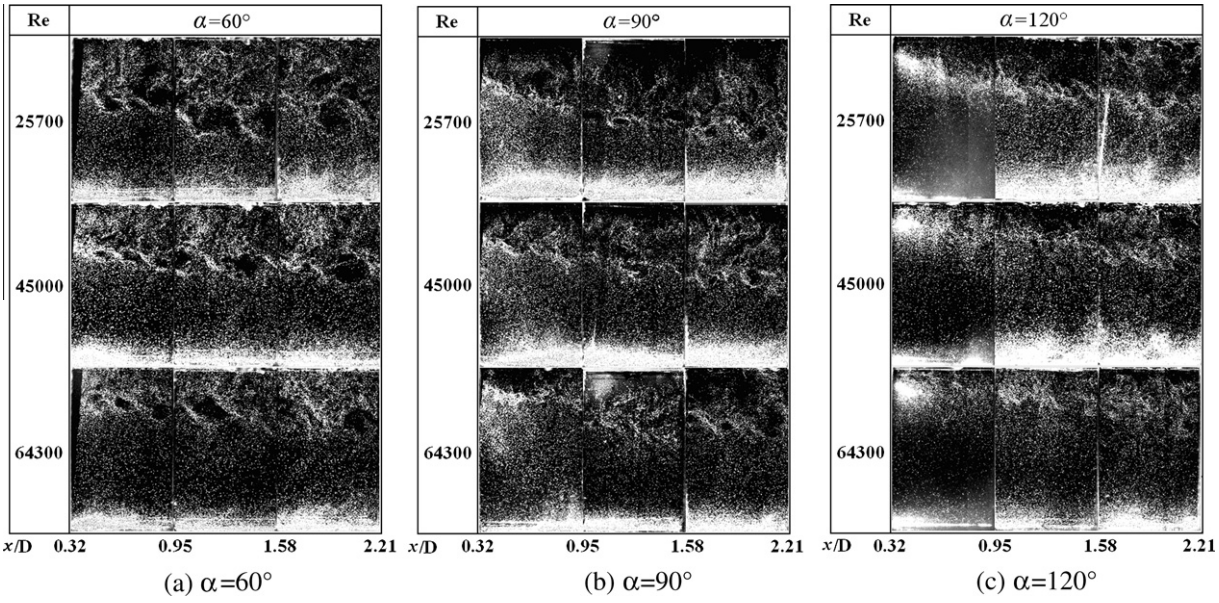

Fig. 8. Instantaneous droplet distributions in the XOY longitudinal section for different crossflow velocities.

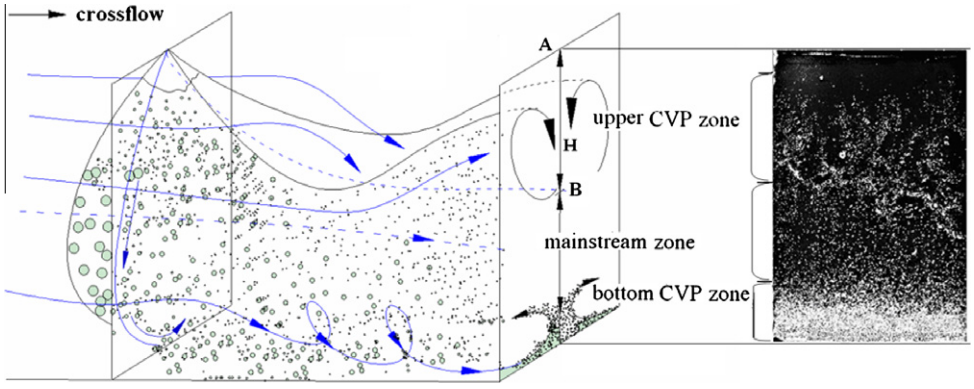

Fig. 9. Schematic drawing of large-scale flow field structures produced by a hollow cone spray into a crossflow.

droplets and the crossflow are intensified. The turbulence of the flow field is enhanced and the droplet dispersion is promoted. On the contrary, when the spray is angled downstream ($\alpha > 90°$), the droplet-crossflow interaction is weakened. The entrained air flow is too weak to carry the droplets and accordingly, the droplet dispersion is inhibited. Fig. 10 shows the spray droplet distribution in different cross-sections along the mixing flow field with $\alpha = 60°$ and $\alpha = 120°$ for Re = 25700. When $\alpha = 60°$, the upper CVP structure is inhibited dramatically because of the coherent structure and the mixing is enhanced significantly. When $\alpha = 120°$, the droplet-wall impingement is more intense and more droplets cluster near the bottom wall, especially in the bottom corners and the bottom CVP zone. The droplets distribute scarcely in the upper portion of the cross sections.

An example of the instantaneous vorticity field of the droplet swarm is shown in Fig. 11 to demonstrate the vortices emerging in the flow field. Due to the gas flow velocity difference between the adjacent zones, the shear layer is caused on the interfaces and then the vortices are induced. Thus, in the central longitudinal section, three obvious vortices occur which are observed to strongly influence the droplet distribution.

The spatial velocity distributions of the spray droplets are shown in Fig. 12 and the comparisons of the velocity and vorticity under different injection angles are given in Fig. 13. Clearly, we can see that the CVP structures have great effects on the droplet velocity distribution. The droplet u-velocity increases to a relatively great value and then decreases in the upper CVP zone; Afterwards, the u-velocity increases gradually to a peak value in the mainstream zone and then decrease again close to the bottom CVP zone where the velocity falls sharply. When the nozzle spray is against the crossflow (e.g. $\alpha = 60°$), the greatest difference between the u-velocity in the upper CVP zone and the mainstream occurs whereas this difference reduces gradually as the injection angle increases (see $\alpha = 90°$ and $\alpha = 120°$). In the upper CVP zone, the

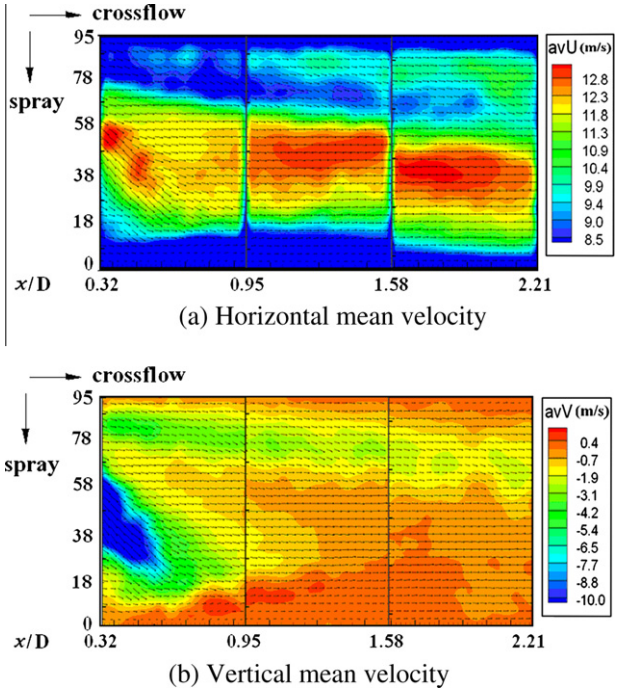

Fig. 12. Spatial distributions of the droplet mean velocity for $\alpha = 90°$, Re = 32100.

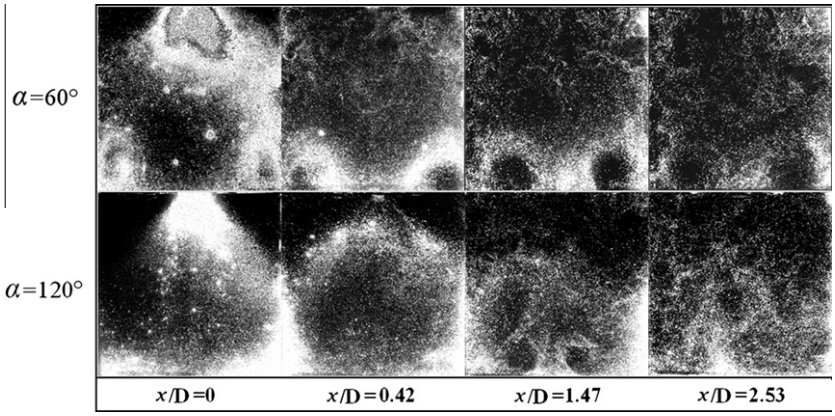

Fig. 10. Droplet distributions in the cross-sections for different injection angles with Re = 25700.

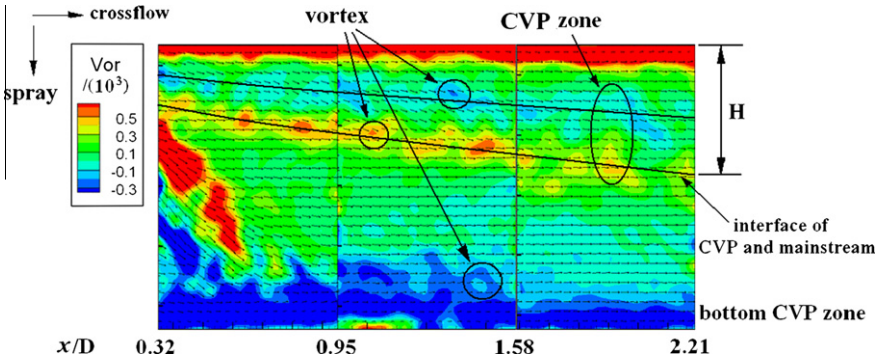

Fig. 11. Spatial distributions of the vorticity of the droplet swarm flow at the XOY longitudinal section for $\alpha = 90°$ (Re = 32100).

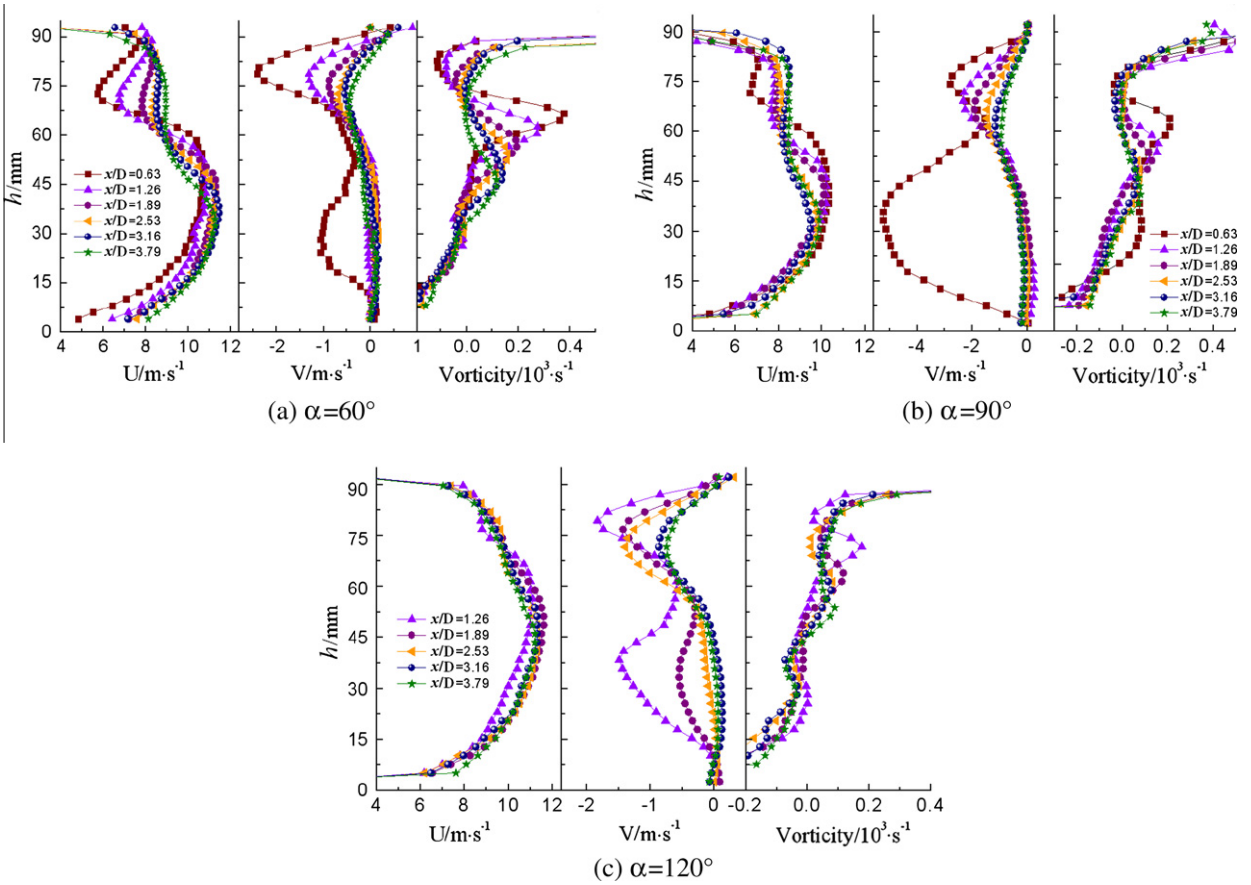

Fig. 13. Time-averaged droplet swarm velocity and vorticity distribution in central section for three injection angles with Re = 25700.

entrained air flows moving downward are caused. The droplets move downward with larger v-velocity and the maximum value occurs with $\alpha = 90°$. It indicates that the strongest entrained air flow is caused when the spray is perpendicular to the crossflow. Furthermore, near the nozzle, the initial spray droplets with large momentum have higher downward speed and can penetrate the mainstream easily. As the mixing develops, these droplets deposit on the bottom wall gradually and at last, the droplet v-velocities are close to 0. The larger vorticity occurs on the shear layers and peaks on the upper shear layer. Along the mixing flow field, the intensity of the upper CVP structure weakens gradually and correspondingly, the differences in different zones decrease for the droplet velocities and vorticity.

Here we define the distance between the top wall and the shear layer on the lower interface of the upper CVP as the depth of the CVP, H, as is shown in Figs. 9 and 11. The depth, H, of the upper CVP under different experimental conditions is shown in Fig. 14. In three cases of the velocity and five of the injection angle, the maximum H/D (the width of the test section, 95 mm) occurs when $\alpha = 90°$ and the minimum occurs when $\alpha = 120°$. This means that the influential area of the upper CVP structure is larger when $\alpha = 90°$. Along the flow field, the depth of the upper CVP increases. These findings agree with the conclusions obtained from the cross-section images of the mixing flow field in our previous experiment. The depth of the upper CVP structures influences the droplet distribution, as can be seen in Fig. 8.

3.2. The coherent structure

It is generally acknowledged that the enhanced entrainment and mixing result from various vertical structures excited in the

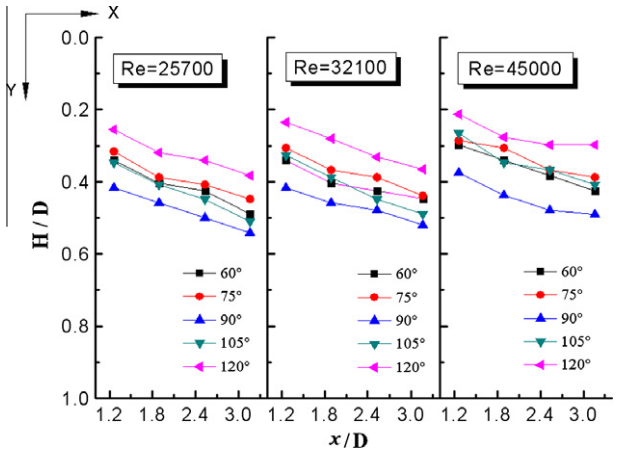

Fig. 14. Comparison of the depth of the upper CVP for different injection angles.

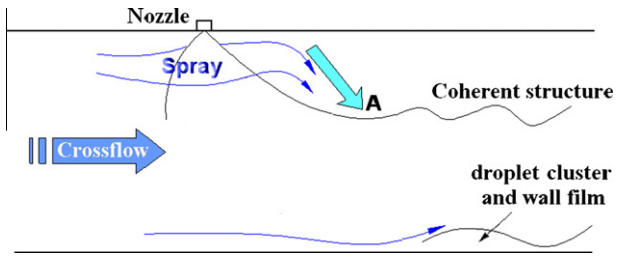

Fig. 15. Schematic drawing of the instantaneous flow field structure in the central cross-section.

two-phase mixing flow field. Studies demonstrate that the dynamic features of the upper CVP are largely responsible for the crossflow mixing under the jet spray conditions. Similarly, according to our experimental images, the upper CVP structure dominates the flow field in the farther downstream. According to the above discussion, the mixing flow field falls into three domains, the upper CVP zone, the mainstream zone and the bottom CVP zone. But the gas flow movement directions in each zone are different. Due to the interactions between the adjacent zones, more complex gas flow movement is induced on their interfaces, and then the dispersion of the droplet becomes more complicated (see Fig. 8).

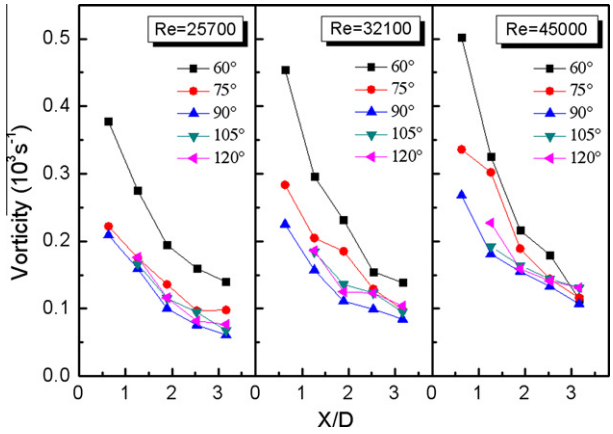

Fig. 16. Vorticity profile in the XOY longitudinal section for different injection angles.

Fig. 15 shows the instantaneous flow field structure in the central cross-section. Due to the lower pressure behind the spray hollow cone [23], a downward gas flow (represented by A in the figure) is induced when a crossflow is introduced into the hollow cone spray system. Because of the difference of the tangential velocity orientation between the gas flow A and the crossflow, the Kelvin–Helmholtz (K–H) instability occurs on their interface (shear layer) due to the shear stress, and then the large-scale coherent structure is induced with the nonlinear effect increasing.

Fig. 16 shows the vorticity profile of the droplet swarm on the interface (shear layer) between the upper CVP and the mainstream in the XOY longitudinal section for different injection angles. Vorticity is the indicator of the intensity of the vortices. Clearly, for the same gas crossflow velocity, the highest vorticity occurs when $\alpha = 60°$ and the lowest when $\alpha = 90°$. The vorticity decreases along the flow field. In addition, for five injection angles, the vorticity has

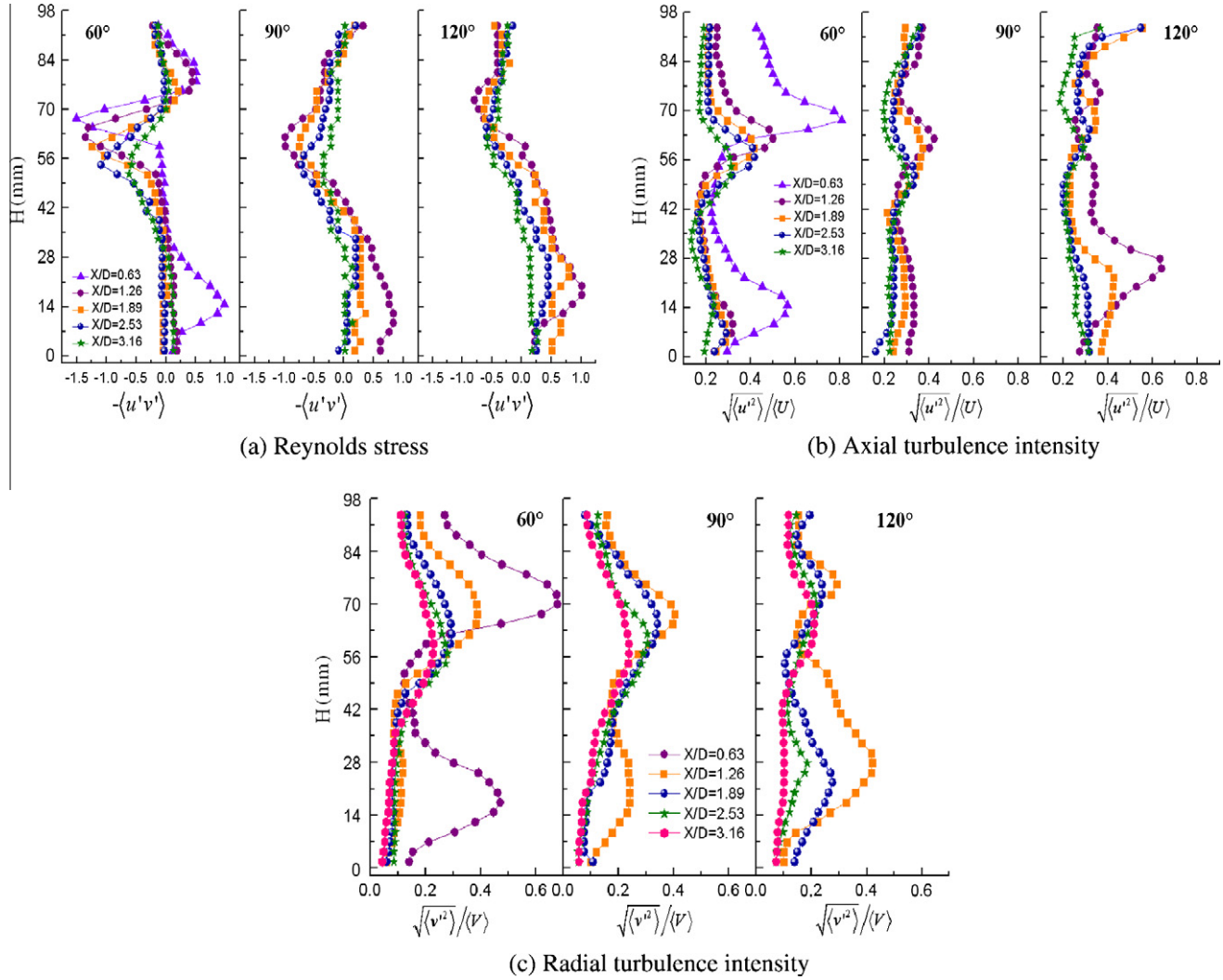

Fig. 17. Profiles of the Reynolds stress, $-\langle u'v' \rangle$, and the axial and radial turbulence intensity, $\sqrt{\langle u'^2 \rangle}/\langle U \rangle$ and $\sqrt{\langle v'^2 \rangle}/\langle V \rangle$, of droplets with different injection angles in the central cross-section (Re = 45,000).

the tendency of enhancement with the crossflow velocity increasing within our experimental velocity range.

Fig. 17 shows the Reynolds stress, $-\langle u'v'\rangle$, and the axial (X-axis direction) and radial (Y-axis direction) turbulence intensity, $\sqrt{\langle u'^2\rangle}/\langle U\rangle$ and $\sqrt{\langle v'^2\rangle}/\langle V\rangle$, of the droplet swarm. Clearly, near the shear layer (the region of the coherent structure), the Reynolds stress (the minus "−" indicates the negative direction of the X-axis) and the axial and radial turbulence intensity decrease along the flow field, which means that the effect on the droplets imposed by the coherent structure reduces gradually. In the mainstream (the middle part of the flow field), they are lower than on the shear layer. The greater values occur when $\alpha = 60^\circ$ and in the same distance their values present a slight decline with $\alpha = 120^\circ$. When $\alpha = 120^\circ$, due to the influence of the initial high-speed spray droplets and the bottom wall, the Reynolds stress, the axial and radial turbulence intensity are all greater than with other injection angles in the lower part.

Hence, also on the basis of the instantaneous droplet distribution of the mixing flow field shown in Fig. 8, we can conclude that the coherent structures on the interface between the upper CVP and the mainstream zone break the stability of the upper CVP structure. When the spray is against the crossflow the larger coherent structures are induced and impose greater influences on the mixing flow field. The turbulence intensity increases and the momentum transfer between the droplets and the crossflow can be enhanced greatly and the dispersion of the droplets is promoted; thus, the mixing is enhanced. Furthermore, the coherent structures prolong the droplet resident time in the mixing and this is beneficial for the two-phase heat and mass transfer in practical high temperature mixing chambers. This finding helps control the mixing of the hollow cone spray into the crossflow to achieve an optimum mixing effect.

4. Conclusions

The flow field of a hollow cone spray into the crossflow in the longitudinal section is investigated experimentally by using PIV visualization system and the image-processing techniques. The instantaneous droplet distributions and the velocity vector fields in the longitudinal direction are obtained. The conclusions are as follows:

(1) In the flow field of a hollow cone nozzle spray into the crossflow, the CVP structures persist for a long time and dominate the mixing flow.
(2) Under the influences of the hollow cone structure of the spray and the wall, the mixing flow field falls into three distinct domains: the upper CVP zone, the mainstream zone and the bottom CVP zone. Their effects on the droplet movement and distribution are different. Due to the existence of the CVP structures, the time-averaged u-velocity of the droplets in the upper CVP zone is lower than that in the mainstream zone, and the strong downward stream is caused in the middle of the two vortices.
(3) Along the flow field, the depth of the CVP increases. For different injection angles, when $\alpha = 90^\circ$, the maximum depth of the CVP occurs.
(4) The coherent structure is generated on the interface between the CVP and the mainstream zone. When the injection angle is against the crossflow ($\alpha < 90^\circ$), the larger coherent structures are induced and impose greater influences on the mixing flow field. The turbulence intensity on the shear layer increases, which results from the greatly enhanced momentum transfer between the droplets and the crossflow, and the dispersion of the droplets is promoted; thus, the mixing is enhanced.

Acknowledgments

The financial supports from the National Nature Science Foundation of China for Creative Research Groups under the Contract No. 51121092 are highly appreciated.

References

[1] P.K. Wu, K.A. Kirkendall, R.P. Fuller, A.S. Nejad, Breakup processes of liquid jets in subsonic crossflows, AIAA Paper 96-3024 13 (1997) 64–73.
[2] T. Inamura, N. Nagai, Spray characteristics of liquid jet traversing subsonic airstreams, J. Propul. Power 13 (1997) 250–256.
[3] S.B. Tambe, S.M. Jeng, H. Mongia, Liquid Jets in Subsonic Crossflow, AIAA Paper 2005-731 (2005).
[4] K.A. Sallam, C.L. Ng, R. Sankarakrishnan, C. Aalburg, K. Lee, Breakup of turbulent and non-turbulent liquid jets in gaseous crossflows, AIAA Paper 2006-1517 (2006).
[5] M. Costa, M.J. Melo, J.M.M. Sousa, Y. Levy, Spray characteristics of an angled liquid injection into subsonic crossflows, J. AIAA 44 (2006) 646–653.
[6] K. Bunce, J.G. Lee, D.A. Santavicca, Characterization of liquid jets-in-crossflow under high temperature, high velocity non-oscillating and oscillating flow conditions, AIAA Paper 2006-1225 (2006).
[7] G.E. Lorenzetto, A.H. Lefebvre, Measurements of drop size on a plain-jet airblast atomizer, J. AIAA 15 (7) (1977) 1006–1010.
[8] H. Eroglu, N. Chigier, Initial drop size and velocity distributions for airblast coaxial atomizers, J. Fluids Eng. 113 (3) (1991) 453–459.
[9] R. Harari, E. Sher, Optimization of a plain-jet airblast atomizer, Atomization and Sprays 7 (1) (1997) 97–113.
[10] R. Harari, E. Sher, Bimodal drop size distribution behavior in plain-jet airblast atomizer sprays, Atomization Sprays 8 (3) (1998) 349–362.
[11] M.Y. Leong, V.G. McDonell, G.S. Samuelsen, Mixing of an airblast-atomized fuel spray injected into a crossflow of air, NASA/CR (2000) 210467.
[12] S. Ghosh, J.C.R. Hunt, Induced air velocity within droplet driven sprays, Proc. R. Soc. Lond. 444 (1994) 105–127.
[13] P.C.H. Miller, M.C. Butler Ellis, C.R. Tuck, Entrained air and droplet velocities produced by agricultural flat-fan nozzles, Atomization Sprays 6 (1996) 693–707.
[14] J.C. Phillips, P.C.H. Miller, N.H. Thomas, Air flow and droplet motions produced by the interaction of flat-fan spray and cross flows, Atomization Sprays 10 (2000) 83–103.
[15] D.P. Schmidt, I. Nouar, P.K. Senecal, C.J. Rutland, J.K. Martin, R.D. Reitz, Pressure-swirl atomization in the near field, SAE Technical (1999) 01–0496.
[16] A. Belhadef, A. Vallet, M. Amielh, F. Anselmet, Pressure-swirl atomization: modeling and experimental approaches, Int. J. Multiphase Flow 39 (2012) 13–20.
[17] C.A. Chryssakis, D.N. Assanis, J.K. Lee, K. Nishida, Fuel Spray Simulation of High-Pressure Swirl-Injector for DISI Engines and Comparison with Laser Diagnostic Measurements, J. Soc. Automot. Eng. (2003) 2003-01-0007.
[18] J.Q. Xue. Computational simulation of flow inside pressure-swirl atomizers, PhD Thesis, University of Cincinnati, 2005.
[19] T. Marchione, C. Allouis, A. Amoresano, F. Beretta, Experimental investigation of a pressure swirl atomizer spray, J. Propul. Power. 23 (5) (2007) 1096–1101.
[20] S. Ghosh, J.C.R. Hunt, Spray jets in a cross-flow, J. Fluid Mech. 365 (1998) 109–136.
[21] S.S. Kachhwaha, P.L. Dhar, S.R. Kale, Experimental studies and numerical simulation of evaporative cooling of air with a water spray – I. Horizontal parallel flow, Int. J. Heat Mass Transfer 41 (1998) 447–464.
[22] S.S. Kachhwaha, P.L. Dhar, S.R. Kale, Experimental studies and numerical simulation of evaporative cooling of air with a water spray – II. Horizontal counter flow, Int. J. Heat Mass Transfer 41 (1998) 465–474.
[23] B.F. Bai, H.B. Zhang, L. Liu, H.J. Sun, Experimental study on turbulent mixing of spray droplets in crossflow, Exp. Therm. Fluid Sci. 33 (2009) (2009) 1012–1020.
[24] B.F. Bai, H.J. Sun, H.B. Zhang, L. Liu, Numerical study on turbulent mixing of spray droplets in crossflow, J. Propul. Power 27 (2011) 132–143.
[25] L. Liu, H.J. Sun, H.B. Zhang, B.F. Bai, Mixing of spray in crossflow in rectangle tube, J. J. Eng. Thermophys. 32 (2) (2011) 231–238.